Development of Automated Identification and Counting Technology for Harmful Algae Using the Flow Imaging Microscope FlowCam

Hirofumi Nakanishi [*1] *Tomoya Itou* [*1]

Species identification and population measurement of underwater microalgae in the fields of water quality and marine environment monitoring rely heavily on manual work performed by skilled operators, posing challenges in terms of accuracy and efficiency. In this study, we have developed an automated identification and counting technology using FlowCam by YOKOGAWA, a flow imaging microscope. Samples of raw water and seawater often contain numerous non-target algae and foreign particles, which are the primary causes of misclassification. To address this issue, a classification support module was introduced to suppress misclassification of non-target data, thereby improving accuracy. Verification targeting the harmful alga Coscinodiscus wailesii in seaweed farming areas demonstrated species identification accuracy of over 95% and a cell density estimation error within ±10%. This technology enables highly accurate and efficient algae monitoring compared to conventional methods and is expected to contribute to applications such as water quality management and red tide prediction.

INTRODUCTION

Dam reservoirs play an important role as a source of drinking water supply. However, mass proliferation of microalgae can cause problems such as filter clogging, odor generation, and deterioration of taste(1). Furthermore, when harmful algae occur in marine areas, they can damage aquaculture and pose risks to human health through seafood consumption(2). For this reason, water quality in such bodies of water is regularly monitored, and measures are implemented to minimize harm through the early identification of harmful algal blooms and toxin production risks.

Current biological water quality surveys employ a method in which samples of raw water and seawater are examined under a microscope in a laboratory, microalgae are classified and counted based on morphological characteristics, and cell density is calculated for each species. As a specific example, a fixed volume of sample water is introduced into a plankton counting chamber fitted with a 1-mm grid, the microalgae within each grid cell are identified to species under the microscope, and the cell count per species is tallied using a counter. Cell density is then calculated by dividing the total count across all grid squares by the volume of sample analyzed(3). However, such methods require considerable effort and long measurement times. They can also be performed only by skilled technicians with specialized knowledge, and measurement accuracy may vary with the technician's judgment.

In response to these challenges, in this study we developed a method for automatically and rapidly identifying and counting microalgae by species using FlowCam, a flow-imaging microscope manufactured by YOKOGAWA. FlowCam continuously images particles in a liquid sample flowing through a flow cell and records and analyzes the resulting images. Figure 1 shows the external appearance of the FlowCam 8000. While the FlowCam 8000 can analyze particle size, shape, and other parameters from acquired images, it does not have a built-in species identification function. Therefore, in this study, we created a learning model from acquired images and developed an artificial intelligence-based species identification technology. Because samples of raw water and seawater contain numerous non-target algae and foreign particles, the primary cause of misclassification, a classification support module was introduced to suppress the misclassification of non-target data and thereby improve accuracy. This paper reports on the development of this technology and the results of verification trials using it to identify and count cells of the harmful alga *Coscinodiscus wailesii* in seaweed farming areas.

*1 DX Business Development Department, Innovation Center, Marketing Headquarters

Figure 1 Exterior appearance of the FlowCam8000

METHODS

System Overview

The system developed in this study begins with comprehensive particle image acquisition and morphological parameter calculation using the FlowCam 8000, with the goal of identifying target algal species and estimating cell density (Figure 2). Although the FlowCam 8000 supports objective lenses ranging from 2× to 20×, a 4× objective lens was used to achieve both image clarity for *C. wailesii* (a cylindrical microalga with a diameter of several hundred μm) and high image acquisition throughput.

Specifically, the FlowCam was used to perform cropping (the process of detecting and extracting each individual particle) and mask generation (the process of extracting a region conforming to the shape of the particle) for each particle, after which morphological parameters were calculated and species identification was carried out. In this verification study, two methods were employed to identify the target species *C. wailesii*: a morphological parameter method that combines morphological parameters calculated by FlowCam with one-class classification, and a deep-learning method that directly trains on cropped particle images. Because field samples may contain particles of non-target species, both methods incorporated an out-of-distribution (OOD) detection mechanism to exclude non-target particles. Here, OOD refers to deviation from the learned distribution, and it was expected that data samples belonging to species other than the target would be detected as OOD. Following identification, cell density C was estimated as

$$C = \frac{N_{acc}}{V \times \eta \times \alpha}, \quad (1)$$

where N_{acc} is the number of particles identified as the target species, V is the volume of processed sample (mL), η is the effective imaging rate (taken as the "Efficiency" value output by the FlowCam software), and α is a correction factor that absorbs instrument-specific variation caused by factors such as partial clipping of particles at the edges of the field of view during imaging. In this study, η = 0.356 and α = 0.760 were used, with cell density expressed in units of cells/mL. Note that α was determined by analyzing the correspondence between cell density obtained through microscopic examination and cell density calculated from FlowCam data in a preliminary validation study, and was calculated based on those results.

Morphological Parameter Method

For morphological parameter method, an effective parameter set was selected from the numerous morphological parameters calculated by VisualSpreadsheet, the dedicated analysis software for FlowCam, through exploratory data analysis examining distributions, correlations, and multicollinearity (Table 1). These parameters summarize information such as size, shape, and texture, consolidating information useful for identification while suppressing noise. To eliminate the effects of scale differences between parameters, standardization was applied prior to training.

A one-class support vector machine[4] (radial basis function [RBF] kernel) was adopted as the model, as it can be trained without negative example data. The framework learns the range of characteristics typical of this species (normal region) from positive example data of *C. wailesii*, treating samples outside that range as non-target. The use of an RBF kernel allows the model to accommodate boundaries that are difficult to express linearly.

Hyperparameters were determined via Bayesian optimization[5]. Specifically, a search was conducted over the two primary parameters, ν and γ, which control outlier tolerance and boundary granularity, respectively, with the

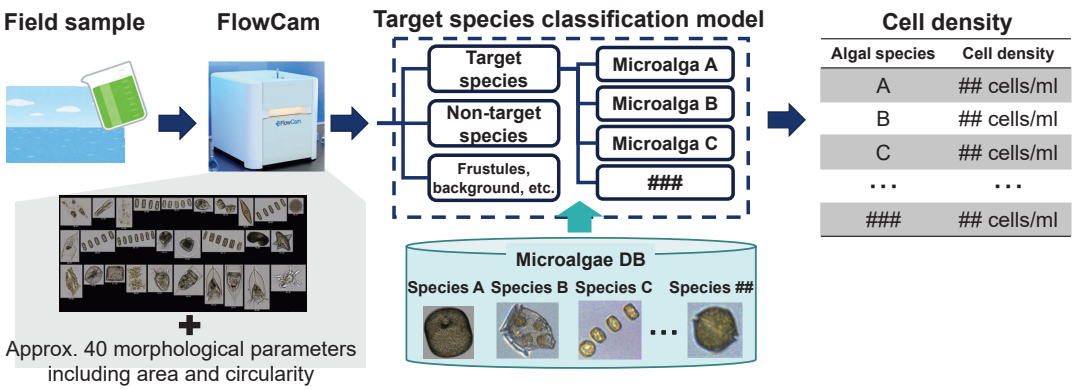

Figure 2 System overview

objective of optimizing the F1 score on the validation data. Since this verification study targets only a single species, *C. wailesii*, the process is completed with the One-Class SVM alone. When targeting multiple species, the method can be extended to a two-stage configuration in which this approach is used as the first stage for outlier detection and candidate extraction, followed by a multiclass classification model in the second stage, thereby enabling identification of multiple target species.

Table 1 Parameters used in the morphological parameter method

Parameter name	Brief description
Aspect Ratio	Ratio of the minor axis to the major axis when the particle is assumed to be an ellipse; values closer to 1 indicate a more circular shape
Compactness	Represents the complexity of the particle; higher values indicate greater complexity
Geodesic Length	Length of the long side when the particle is assumed to be a rectangle
Geodesic Thickness	Length of the short side when the particle is assumed to be a rectangle

Deep-learning Method

The goal of this method was to enhance the robustness of identification when closely related species or unknown particles (non-target species) are present in a sample by extracting high-level features from cropped images of individual particles through a multilayer neural network and thereby capturing local shapes and complex textures that are difficult to characterize using morphological parameters alone. The base model was EfficientNet-V2-Small[6], considering the balance between computational speed and recognition accuracy. As preprocessing, image augmentation techniques adapted to the characteristics of FlowCam images were applied, including resizing, padding, rotation, and contrast/brightness modulation.

Training was structured in two stages. First, high-quality initial representations independent of the target class were acquired through self-supervised learning following the Simple Framework for Contrastive Learning of Visual Representations (SimCLR)[7]. This was followed by a method analogous to supervised contrastive learning (SupCon)[8], through which intra-class compactness and inter-class separation were simultaneously reinforced alongside target species classification training. This process clarified the decision boundary for visually similar particle images, such as those of closely related species, yielding a feature space that enables stable separation. The primary hyperparameters (number of epochs, learning rate, batch size, etc.) were selected via grid search, a method that tests all combinations of specified hyperparameter candidates.

For OOD detection, *k*th nearest neighbor-based OOD detection (kNN-OOD)[9] was adopted, which uses the proximity of features learned by the SupCon encoder. Here, the encoder f_θ refers to the feature-extraction component excluding the classification head (the final fully connected layer, softmax, etc.). A particle image x is mapped to a feature vector $z = f_\theta(x) \in R^d$, and the k-nearest neighbor set $N_k(z)$ based on Euclidean distance with respect to the training feature set Z_{train} is computed. The OOD score $s(x)$ is defined as the mean of the neighbor distances:

$$s(x) = \frac{1}{k} \sum_{z_i \in N_k(z)} \left\| z - z_i \right\|_2$$

A threshold τ was set by multiplying the 95th percentile of the score distribution $\{s(x_j^{val})\}$ on the validation data by a coefficient α (with α = 1.2 in this study), and OOD determination was made according to the following rules:

$$\tau = \alpha \cdot \mathrm{P}_{95}(\{s(x_j^{val})\})$$

$$Decision\ (x) = \begin{cases} in\ distribution & if\ \ s(x) \le \tau \\ out\ of\ distribution & if\ \ s(x) > \tau \end{cases}$$

Here, we used k = 3, with nearest-neighbor search conducted across all training data. Through this approach, an OOD detection mechanism was realized that relies not on the classifier's probability output but on proximity to the distribution of training data, thereby suppressing misclassification when unknown particles are present.

Evaluation Methods

Dataset

To make use of accurately labeled training data, models were constructed using samples from isolated cultures, and evaluation was performed using field seawater samples (Table 2, Figure 3). Culturing was carried out twice, each time with N = 3 (number of samples), with cultivation for 15 days or more and data acquisition using FlowCam every 2 to 3 days. The substantial difference in cell size between the first and second culture samples is attributable to the use of *C. wailesii* strains that differed in their subculture and pre-culture periods. Marine samples were collected from thirty sites in Harima-Nada, Hyogo Prefecture, between September and October 2024. Samples collected from Harima-Nada tended to have smaller cell areas than the cultured samples. Labeling was performed by the microscopic examiner or by individuals working under that examiner's supervision. Additionally, to assess the model's robustness, supplementary marine samples collected off the Tajima coast of Hyogo Prefecture were used

Table 2 Number of images in each dataset

	Culture batch 1	Culture batch 2	Harima-Nada	Off the Tajima coast
C. wailesii	2147	4178	582	5
Partial *C. wailesii*	30	141	—	—
C. wailesii frustules	338	2372	—	—
Species closely related to *C. wailesii*	—	—	193	—
Other (microalgae, debris, etc.)	4528	18176	58247	20245

Figure 3 Example images from each dataset

in the evaluation.

In the deep-learning model, incorporating contrast classes enables stabler construction of the feature space. For this reason, in the present study, several microalgal species morphologically distinct from *C. wailesii*, such as *Anabaena* and *Karenia*, were included in the training data as contrast classes. Note that evaluations were limited to the classification accuracy of *C. wailesii* only.

Evaluation Framework

Seawater samples were collected at 30 sites in Harima-Nada, and after concentrating 10 to 200 mL of raw water according to cell density, imaging was performed using FlowCam. Cell density was estimated using Eq. (1), and samples from off the Tajima coast were evaluated using the same method.

For evaluating classification accuracy, the commonly used metrics Precision, Recall, and F1 score (the harmonic mean of Precision and Recall) were used. Furthermore, to verify the accuracy of cell density estimates, the current microscopy-based cell density calculation method was used as a reference for comparison. For this purpose, the coefficient of determination (R^2) was calculated to evaluate the degree of agreement between estimated and reference values, and mean absolute error (MAE) was calculated to evaluate the magnitude of error. Using these representative evaluation metrics for regression problems, the difference between the present method and the current method was quantitatively assessed.

RESULTS

Comparison of Model Methods

The F1 score of the morphological parameter method was 84.1% (Table 3). Although there were approximately 100-fold more non-target particle images than *C. wailesii* images, misclassification of non-target species was suppressed to approximately 0.25%, preventing a significant drop in Precision (Table 4). Misclassification cases included *C. wailesii* cells with unusually dense pigmentation not represented in the training data, closely related species, and empty frustules and cell debris, some of which were cases that would be difficult even for experts to distinguish (Figure 4).

The F1 score of the deep-learning method was

Table 3 Accuracy metrics for both methods

	Precision	Recall	F1 Score
Morphological parameter method	79.1%	89.9%	84.1%
Deep-learning method	94.3%	91.8%	93.0%

Table 4 Confusion matrix for the morphological parameter method

		Predicted	
		C. wailesii	not *C. wailesii*
Actual	*C. wailesii*	523	59
	not *C. wailesii*	138	58302
	Breakdown		
	Similar species	25	168
	Others	113	58134

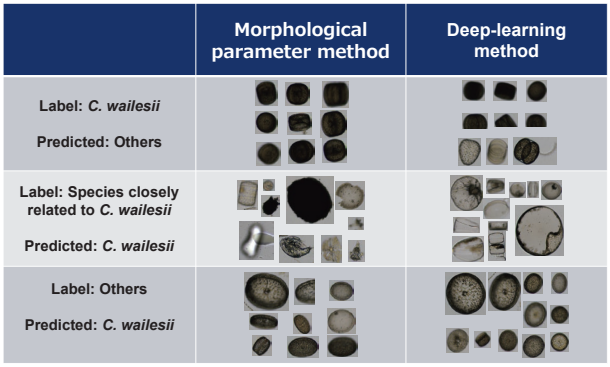

Figure 4 Representative examples of misclassified images from each method

93.0% (Table 3). Misclassification of non-target species was suppressed to approximately 0.05%, with Precision approximately 15% higher and the F1 score approximately 10% higher than the morphological parameter method (Table 5). This can be attributed to the formation of a feature space well-suited to OOD detection through SimCLR/SupCon, and to the suppression of misclassification near the OOD boundary by kNN-OOD detection.

In this verification study, the size of *C. wailesii* differed substantially between the culture data used for training and the Harima-Nada data used for evaluation, with clear differences in cell morphology as well. Despite this, both methods achieved high accuracy sufficient for practical use, suggesting that both approaches appear to successfully model the essential characteristics of *C. wailesii*.

Both methods showed high predictive accuracy ($R^2 \geq 0.9$) and low error (MAE $\approx$ 1.5) relative to the cell density values measured by microscopic counting (Figure 5). This indicates that for species with distinctive morphology such as *C. wailesii*, the morphological parameter method alone may be sufficient to achieve practical accuracy. On the other hand, for species or tasks that rely on complex patterns, fine structures, or localized features, the advantages of the deep-learning method are expected to become more pronounced.

Table 5 Confusion matrix for the deep-learning method

		Predicted	
		C. wailesii	not *C. wailesii*
Actual	*C. wailesii*	534	48
	not *C. wailesii*	32	58408
	Breakdown		
	Similar species	21	172
	Others	11	58236

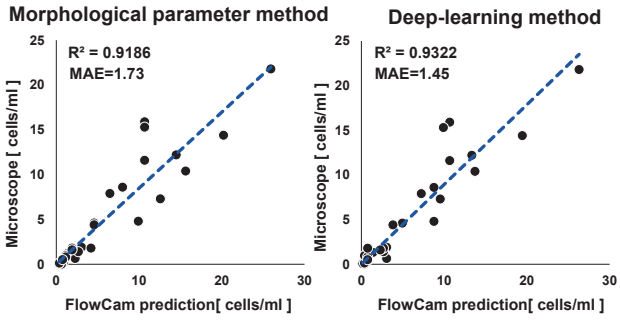

Figure 5 Measured vs. predicted cell density for each method (30 sites)

It is therefore important to select between the two methods according to the required accuracy, the characteristics of the target species, and constraints on processing speed and computational resources.

Robustness Verification of the Deep-learning Method Using Samples from off the Tajima Coast

The accuracy of the deep-learning method, which of the two methods demonstrated superior performance, was verified and its robustness was evaluated using samples collected off the Tajima coast that contained *C. wailesii*. As a result, all particles except one were correctly identified (Table 6, Figure 6). The misclassification case involved a closely related species being identified as *C. wailesii*, and was an image that would be difficult to distinguish even for an expert. These results demonstrate that the method can classify samples from marine areas distinct from those used in model construction, confirming its robustness.

Visualization and Operational Use of OOD Scores in the Deep-learning Method

In the deep-learning method, OOD detection is performed using an OOD score based on the mean kNN distance in the model's embedding space. Because SupCon trains the embedding space such that samples within the same class are placed close together while samples from different classes are placed far apart, the OOD score quantifies the degree of separation from known classes. When the OOD score distribution of images estimated to be *C. wailesii* was actually observed, the proportion of non-target species images increased as the score rose, with a sharp change in trend around the set threshold (Figures 7 and 8). Furthermore,

Table 6 Confusion matrix for the Tajima coast data

		Predicted	
		C. wailesii	not *C. wailesii*
Actual	*C. wailesii*	5	0
	not *C. wailesii*	1	20244

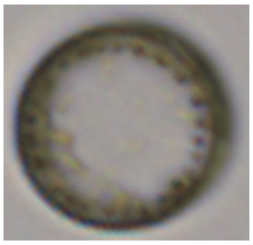

Figure 6 A misclassified *C. wailesii* image from the Tajima coast data

since cases near the threshold frequently involved closely related species, high accuracy, stability, and transparency can be achieved in practice by applying a workflow in which only data near the threshold is manually reviewed, thereby suppressing misclassification of non-target species. In addition, continuous improvement of the model becomes possible by accumulating human judgment results for cases near the threshold and using them for retraining.

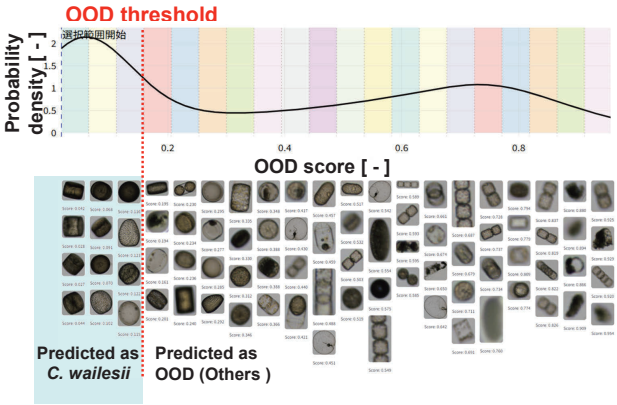

Figure 7 Example images at various OOD scores

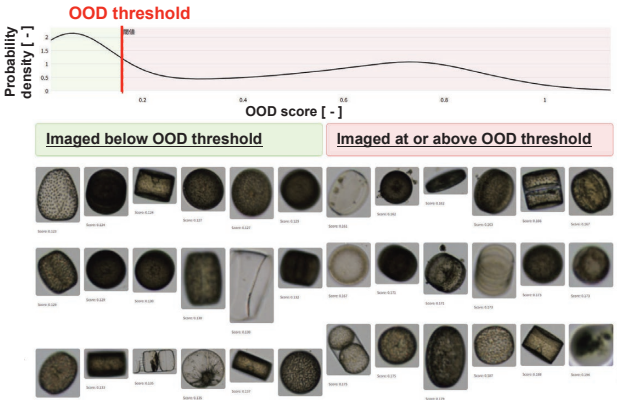

Figure 8 Images around the OOD threshold

DISCUSSION

In this study, we developed and evaluated two methods for identifying specific microalgal species using FlowCam, a morphological parameter method and a deep-learning method. Although the deep-learning method achieved higher accuracy, both methods demonstrated sufficient accuracy for practical applications. Each method offers distinct advantages in terms of accuracy and computational load, so complementary deployment of both methods according to field requirements would be an effective approach. The morphological parameter method is the stronger option in situations where computational resources or ease of implementation are limiting factors, while the deep-learning method is advantageous in environments with frequent occurrences of closely related species, distributional variability due to season or geographic area, and frequent observation of unknown particles. In addition, the deep-learning method can simultaneously achieve exceptionally high accuracy and continuous model improvement through partial human intervention using OOD scores. In future scenarios requiring simultaneous identification of multiple species or extension to colonial species, the advantages of the deep-learning method are expected to become even more pronounced.

CONCLUSION

In this study, we developed an automated species identification and counting technology for microalgae using the flow imaging microscope FlowCam, demonstrating the potential to realize algae monitoring that is both faster and more accurate than conventional methods based on microscopic observation by skilled technicians. Going forward, we plan to address the verification of accuracy and robustness when this technology is applied to multiple other species, as well as the development of cell identification and counting technology for colonial species.

ACKNOWLEDGMENTS

This research was conducted in collaboration with the Fisheries Technology Institute of the Hyogo Prefectural Technology Center for Agriculture, Forestry and Fisheries. We would like to express our gratitude to all those who provided their cooperation.

REFERENCES

(1) Ministry of Land, Infrastructure, Transport and Tourism, Guidelines for Improving Water Quality in Dam Reservoirs, 2018 (in Japanese)
(2) K. Kohata, “Basic Knowledge on Environmental Issues: Red Tide,” National Institute for Environmental Studies News, Vol. 23, No. 4, 2004, pp. 8-9 (in Japanese)
(3) Japan Water Works Association, Standard Methods for Examination of Water, 2011 Edition, Part VI: Biology, 2011 (in Japanese)
(4) B. Schölkopf, R. C. Williamson, et al., “Support Vector Method for Novelty Detection,” Proc. Advances in Neural Information Processing Systems (NeurIPS), Vol. 12, 2000, pp. 582-588
(5) J. Snoek, H. Larochelle, et al., “Practical Bayesian optimization of machine learning algorithms,” Proc. Advances in Neural Information Processing Systems (NeurIPS), Vol. 25, 2012, pp. 2951-2959
(6) M. Tan, Q. V. Le, “EfficientNetV2: Smaller Models and Faster Training,” Proc. 38th Int. Conf. Machine Learning (ICML), Vol. 139, pp. 10096-10106
(7) T. Chen, S. Kornblith, et al., “A Simple Framework for Contrastive Learning of Visual Representations,” Proc. 37th Int. Conf. Machine Learning (ICML), Vol. 119, 2020, pp. 1597-1607
(8) P. Khosla, P. Teterwak, et al., “Supervised Contrastive Learning,” Proc. Advances in Neural Information Processing Systems (NeurIPS), Vol. 33, 2020, pp. 18661-18673
(9) Y. Sun, Y. Ming, et al., “Out-of-Distribution Detection with Deep Nearest Neighbors,” Proc. 39th Int. Conf. Machine Learning (ICML), Vol. 162, 2022, pp. 20827-20840